

Temperature-dependent shifts of three emission bands for ZnO nanoneedle arrays

Bingqiang Cao, Weiping Cai,^{a)} and Haibo Zeng

Key Lab of Materials Physics, and Anhui Key Laboratory of Nanomaterials and Nanostructures,
Institute of Solid State Physics, Chinese Academy of Sciences, Hefei 230031, Anhui,
People's Republic of China

(Received 7 November 2005; accepted 18 March 2006; published online 17 April 2006)

The photoluminescence properties of ZnO nanoneedle arrays, grown on silicon substrate by electrodeposition, are studied over the temperatures from 10 K to 300 K. There exist three emission bands in ultraviolet, violet, and green regions, respectively. With increasing temperature, these bands show different temperature dependences: A normal redshift for the ultraviolet emission, S-shaped shift for the violet emission, and blueshift for the green one. The origins of these three bands and their temperature-dependent shifts are explained based on defect levels (zinc interstitial and oxygen vacancy levels) and carrier localization effect at the defect levels in addition to band-gap shrinkage. © 2006 American Institute of Physics. [DOI: 10.1063/1.2195694]

Ultraviolet (UV) or blue light-emitting wide-band-gap semiconductors have the potential to revolutionize the display, illumination, and information storage systems in the near future. In addition to typical direct transition semiconductors GaN (3.39 eV) and ZnSe (2.70 eV), ZnO is another one with a band gap of 3.37 eV and a high exciton bound energy of 60 meV at room temperature (RT), which is higher than the values of GaN (26 meV) or ZnSe (20 meV) and also higher than the RT thermal energy (25 meV). The stable excitons could lead to more efficient UV light-emitting even laser actions.¹ Besides its UV light-emitting properties, visible luminescence in range of 400–700 nm for ZnO has also been widely studied because of its potential applications in low-voltage field emissive display.² Although luminescence properties have been the subject of ZnO studies for several decades,³ the emission centers and mechanisms are still controversial^{4–11} due to their complexity and sensitivity to the surface states, mirror changes of electronic configurations, and preparation methods. Many controversial viewpoints were presented about the origin of the ordinary green emission around 520 nm.^{7–10} As for the violet (around 410 nm) and red emission (around 600 nm) bands, there are only few discussions without more evidence.^{11,12} So, a full understanding of the different luminescence emissions has been being a challenging and significant subject in the ZnO emission studies.

In this letter, we report the photoluminescence (PL) spectra of ZnO nanoneedle arrays, which are prepared by a template-free electrochemical deposition method on a silicon substrate, from 10 K to 300 K over a wide energy range from 1.7 eV to 3.5 eV, and study the dependences of different emission bands on temperature. There exist three emission bands in the UV, violet, and visible regions, respectively, which show different temperature dependences. The UV emission band shows a normal redshift with the increasing temperature, while the violet and green emission bands exhibit anomalous S-shaped and monotonic blueshifts, respectively.

The ZnO nanoneedle arrays used in this study were grown on a (111)-oriented gold film-coated silicon substrate by electrochemical deposition method, as previously described in detail in Ref. 13. PL spectra (in the range of 1.7 eV–3.5 eV) over a temperature range from 10 K to 300 K were recorded under excitation with 267 nm light of a 10 mW quasi-continuous-wave Ti: Sapphire laser. Electron paramagnetic resonance (EPR) (EPR-200, 9.5GHz) and X-ray photoelectron spectrum (XPS) (WSCALAB MKII) were also measured at RT to detect the defect states existing in the samples.

Figure 1 shows the typical morphology of the ZnO nanoneedle array, which is similar to that previously reported.¹⁵ The products consist of straight nanowires with needlelike tips and exhibit a well-aligned array on the substrate perpendicularly. The corresponding x-ray diffraction pattern shows two peaks from ZnO sample: A very strong (002) peak and a very weak (004) peak, indicating that the ZnO nanoneedle array has c-axis orientation and good alignment along the normal direction of the substrate, as shown in Fig. 1.

Figure 2(a) demonstrates the PL spectra in the region from 1.7 eV to 3.5 eV measured at the temperatures from 10 K to 300 K. There are two distinct peaks situated at the green (about 2.2 eV) and UV (about 3.3 eV) regions, respectively, and one unobvious band superimposed between them for all spectra. With increasing temperature, the UV peak shows an obvious redshift, but the green peak blueshifts and its relative intensity to UV peak decreases. Further analyses have revealed that all spectra can be well fitted by

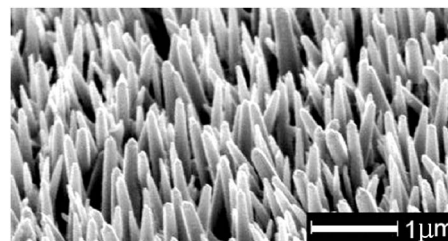


FIG. 1. Field emission scanning electron microscopy image of the as-prepared sample.

^{a)} Author to whom correspondence should be addressed; electronic mail: wpcai@issp.ac.cn

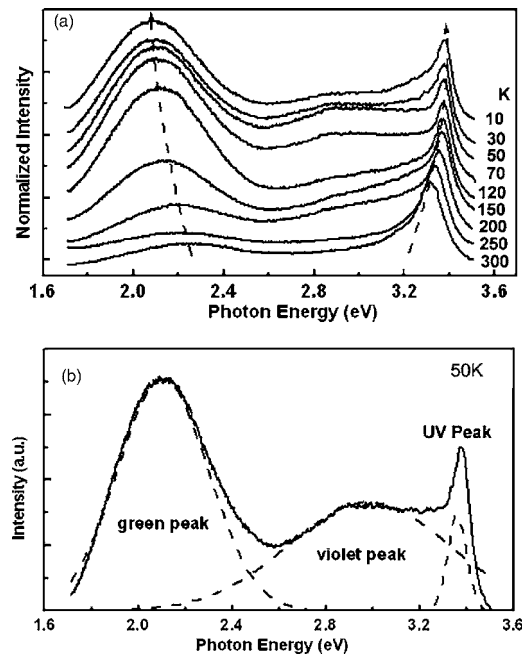


FIG. 2. PL spectra of the as-prepared sample. (a) PL spectra at different temperatures (all spectra are normalized by the UV peak intensity and shifted in the vertical direction for clarity). (b) Typical Gaussian-fitting analysis of the PL spectrum at 50 K (correlation coefficients: 0.99).

three Gaussian peaks. The correlation coefficients are up to 0.99. The unobvious band between the green and the UV peaks is mainly contributed from a violet (about 3.1 eV) emission. Figure 2(b) gives a typical Gaussian analysis result for the full PL spectrum of 50 K, where a violet emission band is illustrated. The Gaussian-fitted violet emission bands from 10 K to 300 K are shown in Fig. 3(a). With temperature increases, the peak intensity decreases, as we usually expect. But, the peak position shift shows a different style from the other two peaks. As the temperature increases from 10 K to 70 K, the violet peak redshifts by 35 meV, which is much larger than the band-gap shrinkage value over this temperature range predicted by Varshni formula¹⁴ (4 meV, see the following paragraph). If the temperature increases from 70 K to 150 K, however, the peak blueshifts by about 160 meV without considering the band-gap shrinkage of 11 meV in this temperature range. A further increase to RT induces the peak to redshift again by 31 meV, that is similar to the prediction of the Varshni formula in this temperature range. In other words, the violet emission shows an *S*-shaped (or red-blue-red) shift with an increase in temperature, as exhibited in Fig. 3(b).

For the UV emission of a ZnO crystal, it is usually attributed to the interband recombination of electrons and holes in form of excitons. Generally, due to the temperature-induced lattice dilatation and electron-lattice interaction, the interband emission peak energy follows the well-known Varshni formula:¹⁴

$$E_g(T) = E_g(0) - \alpha \cdot T^2 / (T + \beta), \quad (1)$$

where $E_g(T)$ is the band gap at an absolute temperature T , and α, β are the Varshni thermal coefficients related with given materials. The solid line in lower frame of Fig. 3(b) denotes the fitting results by Eq. (1) for the UV emission from 10 K to 300 K. The obtained fitting parameters of E_0 , α , and β are 3.379 eV, 7.5×10^{-4} eV/K, and 1050 K, re-

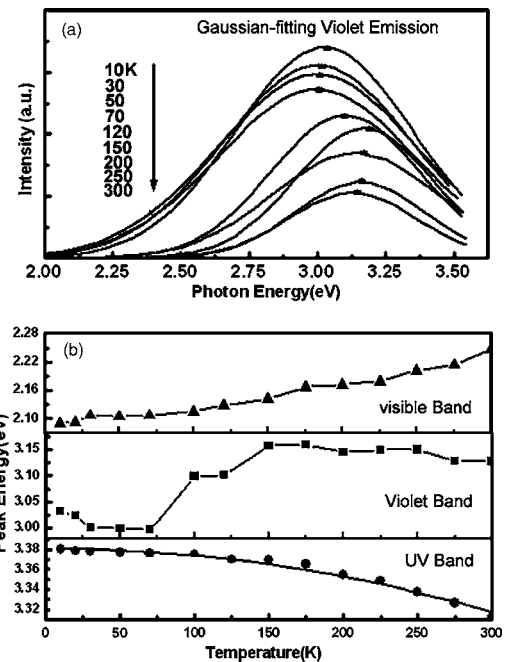


FIG. 3. (a) Gaussian-fitted violet emission bands at different temperatures. (The curves from top to bottom correspond to the temperatures shown in the left, respectively.) (b) The temperature-dependent peak position for the three emission bands. (Dash-line: aid to eyes; Solid line: fitting result by Varshni formula).

spectively, which are comparable to the values reported in ZnO films.¹⁵ So the redshift with rising temperature for the UV emission proves its excitonic origin.

The visible (green and violet) bands show anomalous temperature-dependent behaviors, which differ remarkably from the monotonous band-gap shrinkage with increasing temperature. Therefore, they could be associated with the defect-related levels in the ZnO nanoneedles. EPR and XPS spectral measurements were thus conducted. The EPR spectrum of the as-prepared sample shows a clear signal with $g = 1.96$ (not shown here). Although this EPR signal was formerly attributed to the singly ionized oxygen vacancy V_o^+ ,⁹ it has been unambiguously proven that this signal is typically associated with shallow donors,^{8,9,16} and its position appears to be independent of the shallow donor identity, such as, intrinsic Zn_i (Refs. 8 and 16) or doped copper.⁹ The full XPS spectrum (not shown here) indicates that there is no any other impurity detected than the Zn, O, adsorbed carbon, and gold (from the Au/Si substrate) signals. So the EPR signal with $g = 1.96$ in the nanoneedle sample corresponds to the Zn_i shallow donors, which has a 0.22 eV energy gap below the conduction band.¹⁷ Moreover, the O 1s peak analysis in the high-resolution XPS spectrum proves the relatively higher concentration of oxygen-deficient states in the nanoneedle surface layer, which is a deep level situated 0.9 eV above the valence band.¹⁸

Based on these two existing defect levels in the ZnO nanoneedles and the similar temperature-induced *S*-shaped shift behavior observed in ternary or quaternary nitride semiconductors, such as, InGaN,¹⁹ AlGaN,²⁰ and GaInNAs,²¹ which are closely related to the carrier localization caused by alloy composition or inhomogeneities,¹⁹⁻²² we believe that the violet emission (3.03 eV at 10 K) is from exciton recombination between the electrons localized at the Zn_i -shallow donor levels and holes in the valence band, as shown in Figs.

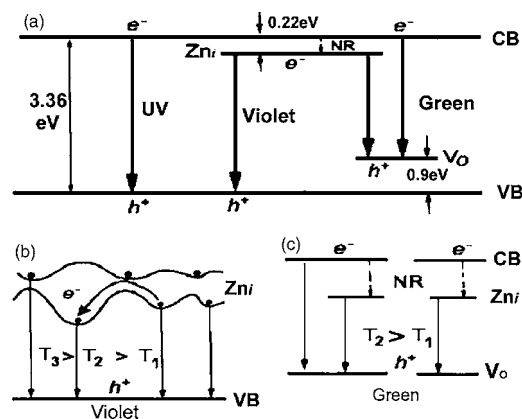


FIG. 4. (a) Schematic illustration of the ZnO band structure and the proposed UV, violet, and green emission processes, NR: Nonradiative transition. (b) Model of the localized electrons at Zn_i defect levels and their transition process with increasing temperature. (c) Model of the green emission with increasing temperature.

4(a) and 4(b). Its emission energy is consistent with the theoretical value between these two levels.²² As the temperature increases from 10 K to 70 K, a redshift appears because the excitons gain in thermal energy sufficiently to overcome small energy barriers and are trapped in adjacent lower levels of the localized states from where the recombination takes place [T_2 process in Fig. 4(b)]. Obviously, this redshift also includes the contribution from the temperature-induced band-gap shrinkage of 4 meV. The following blueshift of 160 meV at the temperature from 70 K to 150 K is caused by the thermal population of electrons localized at higher-energy states, and transitions from these higher levels to the valence band [T_3 process in Fig. 4(b)]. In this temperature range, the influence of band-gap shrinkage is totally counteracted by the localization effect. At temperatures over 150 K, the shift of the emission band is mainly determined by the behavior of the band-gap shrinkage, and the shift energy is in accordance with the value of the Varshni relation prediction. Therefore, the S -shaped shift of the violet emission is the result of competition between the temperature-induced localization effect and band-gap shrinkage.

As for green emission, theoretical studies have identified the electron-hole radiative recombination at the V_o center as a source of the green luminescence.¹⁸ However, its proper transition process is still not very clear now. Considering its monotonous blueshift and decreasing relative intensity with increasing temperature, here, we believe that the green emission at near RT is composed of two transitions: From the conduction band to V_o levels and from Zn_i levels to V_o levels, as shown in Figs. 4(a) and 4(c). In fact, the existence of these two types of transitions have been confirmed by optically detected EPR experiments, respectively.^{23,24} With decreasing temperature, more electrons in conduction band first relax to lower Zn_i levels nonradiatively, and then recombine with holes at V_o levels, which results in the green emission shift to lower energy with narrower full width at half maximum, changing from 600 meV at 300 K to 400 meV at 50 K. Correspondingly, the green and violet emission intensities, compared with that of UV emission, are increased since more electrons at the Zn_i levels recombine with holes at oxygen vacancy and in valence band.

In summary, we have investigated the PL properties of ZnO nanoneedle array, prepared by electrochemical deposition method, over the temperature range from 10 K to 300 K. The UV, violet, and green emission bands exhibit red-, S -shaped, and blueshifts, respectively, with increasing temperatures. The redshift of UV exciton emission is from the temperature-induced band-gap shrinkage. The violet emission is attributed to electron-hole recombination between the Zn_i defect level and valence band, and its S -shaped shift is a result of competition between electron localization effect at Zn_i level and band-gap shrinkage. The monotonic blueshifted green emission is attributed to two temperature-related transitions between the conduction band, Zn_i , and V_o levels.

This work was financially supported by National Natural Science Foundation of China (Grant No. 50271069) and the National Project for Basic Research (Grant No. 2006CB300402). The authors thank Dr. Changhui Ye for his helpful discussion and Dr. Xinjian Xie for his kind technical assistance with the PL measurements.

¹X. D. Wang, C. J. Summers, and Z. L. Wang, *Nano Lett.* **4**, 423 (2004); M. H. Huang, S. Mao, H. Feick, H. Q. Yan, Y. Y. Wu, H. Kind, E. Weber, R. Russo, and P. D. Yang, *Science* **292**, 1897 (2002).

²V. W. Leverenz, *An Introduction to Luminescence of Solids* (Dover, New York, 1968).

³D. G. Thomas, *J. Phys. Chem. Solids* **15**, 86 (1960).

⁴W. Shan, W. Walukiewicz, J. W. Ager III, K. M. Yu, H. B. Yuan, H. P. Xin, G. Cantwell, and J. J. Song, *Appl. Phys. Lett.* **86**, 191911 (2005).

⁵V. A. Fonoberov and A. A. Balandin, *Appl. Phys. Lett.* **85**, 5971 (2004).

⁶D. Li, Y. H. Leung, A. B. Djurišić, Z. T. Liu, M. H. Xie, S. L. Shi, S. J. Xu, and W. K. Chan, *Appl. Phys. Lett.* **85**, 1601 (2004).

⁷K. Vanheusden, C. H. Seager, W. L. Warren, D. R. Tallant, and J. A. Voigt, *Appl. Phys. Lett.* **68**, 403 (1996).

⁸A. B. Djurišić, W. C. H. Choy, V. A. L. Roy, Y. H. Leung, C. Y. Kwong, K. W. Cheah, T. K. G. Rao, W. K. Chan, H. F. Lui, and C. Surya, *Adv. Funct. Mater.* **14**, 856 (2004).

⁹N. Y. Garces, L. Wang, L. Bai, C. N. Giles, L. E. Halliburton, and G. Cantwell, *Appl. Phys. Lett.* **81**, 622 (2002).

¹⁰D. C. Reynolds, D. C. Look, B. Jogai, and H. Morkoç, *Solid State Commun.* **101**, 643 (1997).

¹¹J. F. Xu, J. R. Zhang, W. P. Ding, W. Yang, Y. W. Du, J. Zuo, C. Y. Xu, Y. H. Zhang, and Z. L. Du, *Solid State Commun.* **101**, 467 (1997).

¹²L. E. Greene, M. Law, J. Goldberger, F. Kim, J. C. Johnson, Y. Zhang, R. J. Saykally, and P. Yang, *Angew. Chem., Int. Ed.* **42**, 3031 (2003).

¹³B. Q. Cao, W. P. Cai, G. T. Duan, Y. Li, Q. Zhao, and D. P. Yu, *Nanotechnology* **16**, 2567 (2005).

¹⁴Y. P. Varshni, *Physica (Amsterdam)* **34**, 149 (1967).

¹⁵H. J. Ko, Y. F. Chen, Z. Zhu, T. Yao, I. Kobayashi, and H. Uchiki, *Appl. Phys. Lett.* **76**, 1905 (2000).

¹⁶D. C. Look, J. W. Hemsky, and J. R. Sizelove, *Phys. Rev. Lett.* **82**, 2552 (1999).

¹⁷E. G. Bylander, *J. Appl. Phys.* **49**, 1188 (1978).

¹⁸S. B. Zhang, S. H. Wei, and A. Zunger, *Phys. Rev. B* **63**, 075205 (2001).

¹⁹P. G. Eliseev, P. Perlin, J. H. Lee, and M. Osiński, *Appl. Phys. Lett.* **71**, 569 (1997).

²⁰Y. H. Cho, G. H. Gainer, A. J. Fischer, and J. J. Song, S. Keller, U. K. Mishra, and S. P. Denbaars, *Appl. Phys. Lett.* **73**, 1370 (1998).

²¹L. Grenouillet, C. Bru-Chevallier, G. Guillot, P. Gilet, P. Duvaut, C. Vannuffel, A. Million, and A. Chenevas-Paule, *Appl. Phys. Lett.* **76**, 2241 (2000).

²²Q. Li, S. J. Xu, M. H. Xie, and S. Y. Tong, *J. Phys.: Condens. Matter* **17**, 4853 (2005).

²³L. S. Vlasenko and G. D. Watkins, *Phys. Rev. B* **71**, 125201 (2005).

²⁴F. H. Leiter, H. R. Alves, A. Hofstaetter, D. M. Hofmann, and B. K. Meyer, *Phys. Status Solidi B* **226**, R4 (2001).